Volume 1 | Number 1 | Jan 2013 | Pages 1–100

ChemComm

Chemical Communications
www.rsc.org/chemcomm

ROYAL SOCIETY OF CHEMISTRY

ROYAL SOCIETY OF CHEMISTRY

www.rsc.org/chemcomm

ChemComm

COMMUNICATION

Nanostructured SnS–N-doped graphene as an advanced electrocatalyst for the hydrogen evolution reaction

S.S. Shinde, Abdul Sami, Dong-Hyung Kim, Jung-Ho Lee*

The hydrogen evolution reaction (HER) via water splitting requires the development of advanced and inexpensive electrocatalysts to replace expensive platinum (Pt)-based catalysts. Scalable hydrothermal synthesis of SnS on N-reduced graphene (N-rGr) sheets is presented for the first time, as a candidate for highly-active electrocatalysts with long-term stability in acidic, neutral, and alkaline media. This hybrid catalyst reveals a low overpotential of -125 mV, Tafel slope of 38 mV/dec, exchange current density of 6.23 mA/cm^2, onset potential of 59 mV, and long-term durability.

Introduction

Hydrogen is a clean, efficient, renewable, zero-emission and durable energy carrier and has been intensively pursued to mitigate the global issues of increasing energy scarcity and environmental deterioration.[1] The production of sustainable hydrogen has motivated an intense search for effective electrocatalysts suitable for the hydrogen evolution reaction (HER).[2] Presently, platinum (Pt) and Pt-based carbon catalysts are the most efficient heterogeneous HER catalysts; however, the high-cost and slow HER kinetics of Pt-based metals hamper their commercialization.[3] Thus, the replacement of Pt with earth-abundant metals would facilitate the global scalability of such potential clean-energy technologies.

To date, a variety of non-noble materials have been investigated for catalyzing the electrochemical HER, including metal sulfides,[4] hydroxides (oxides),[5] nitrides,[6] borides,[7] phosphides,[8] carbides[9] and complexes.[10] For natural hydrogenase systems, metal sulfur clusters with five permanent ligands in a distorted octahedral ligation shell have been shown to be the active sites for HER.[11] Many efforts have been aimed toward preparation of inorganic metal sulfur complexes analogous to these biological active sites. Several metal complexes, including MoS$_2$, Mo$_2$C, WS$_2$, NiS, TiN and CoS$_2$, have also been identified as active HER catalysts in both acidic and alkaline solutions.[12] Compared to other inorganic materials, tin sulfides, which include several compounds such as SnS, SnS$_2$, Sn$_2$S$_3$, Sn$_3$S$_4$ and Sn$_4$S$_5$, have attracted more attention owing to their structural multiformity, low cost, unexpected catalytic activity, and high electrical conductivity in lithium batteries, solar cells and catalysis.[13] To the best of our knowledge, no research on the use of SnS as HER catalyst has yet been reported.

The present work shows nanoscale SnS to be a capable electrocatalyst for the HER due to the exposure of numerous active edge sites. Confinement of nanoparticles within conducting carbon materials, such as graphene and carbon nanotubes,[14] has proven effectual in limiting the size of particles to the nanometer scale, thus improving their HER performance due to strong chemical/electrical coupling. However, graphene-based composite electrodes often suffer from the following major issues, i.e., poor stability, low mass activity by the weak bonding of the catalysts–graphene, a high mass density of the loaded noble metal and oxide catalysts, and the ineffective packing of 2D graphene sheets. Chemical engineering of pristine graphene by substitution of heteroatoms, e.g., N, P, S, and Se, is an effective way to tailor its electronic structure and electrochemical properties.[2,15] Realistic design of low-cost bulk quantities of SnS with carbon materials as large-scale HER catalysts could lead to a new series of catalytic materials for practical use.

Here we report the first scalable synthesis of SnS on N-reduced graphene (N-rGr) sheets and demonstrate high HER electrocatalytic activity of the resulting SnS/N-rGr hybrid with low onset overpotential and small Tafel slopes. Graphene sheets are believed to play a pivotal role in the hybrid by providing functional groups for strong coupling with SnS precursors, acting as an internment environment for SnS nucleation and growth, and providing a charge transport pathway for high electrocatalytic activity. In addition, we investigated the long-term stability of the SnS/N-rGr hybrid in acidic, neutral and basic media. A possible catalytic mechanism of the HER is also explained.

Results and discussion

SnS/N-rGr hybrids were synthesized using a low-temperature solution-phase reaction of tin chloride and sodium sulfide in N,N-dimethylformamide (DMF), ethylene glycol (EG) and hydrazine suspension of thermally exfoliated N-graphene (N-Gr), followed by a high-temperature (180 °C) hydrothermal process for crystallization of the SnS/N-rGr catalysts and reduction of graphene, as shown in Fig. 1a (see the ESI for detailed experimental procedure, Fig. S1a). Figures 1 b and d show scanning electron microscopy (SEM) images of the resulting SnS/N-rGr hybrid and SnS nanoparticles, respectively. Transmission electron microscopy (TEM, inset of Fig. 1b) revealed that the SnS/N-rGr catalyst exhibited a well distributed SnS nanosheet morphology interrelated with N-rGr. In contrast, in the absence of N-rGr, the identical synthesis method (Fig. 1c) produced SnS coalesced into 3D-like particles of various

Department of Materials and Chemical Engineering, Hanyang University, Ansan, Kyunggido, 426-791, Republic of Korea. E-mail: jungho@hanyang.ac.kr, Phone: +82-31-400-5278, Fax: +82-31-419-7203

sizes (Fig. 1d). The TEM image (Fig. 2a) showed that most of the SnS nanosheets were homogenously dispersed on the N-graphene, with some possessing folded edges exhibiting parallel lines corresponding to the different layers of the SnS sheets (Fig. 2a inset). High-resolution TEM revealed orthorhombic atomic lattices in the SnS basal planes and plentiful open edges of the

nanoparticles (Fig. 2b). The interatomic distances determined TEM corresponded to the (101), (210), (111), and (411) planes. The were well matched with the X-ray diffraction (XRD) pattern (Fig. 2c which confirmed the orthorhombic crystal structure (JCPDS: 073-1859) of the prepared SnS/N-rGr hybrid. Figure S1b shows th different plane orientations of SnS unit cell with Pbnm symmetry.
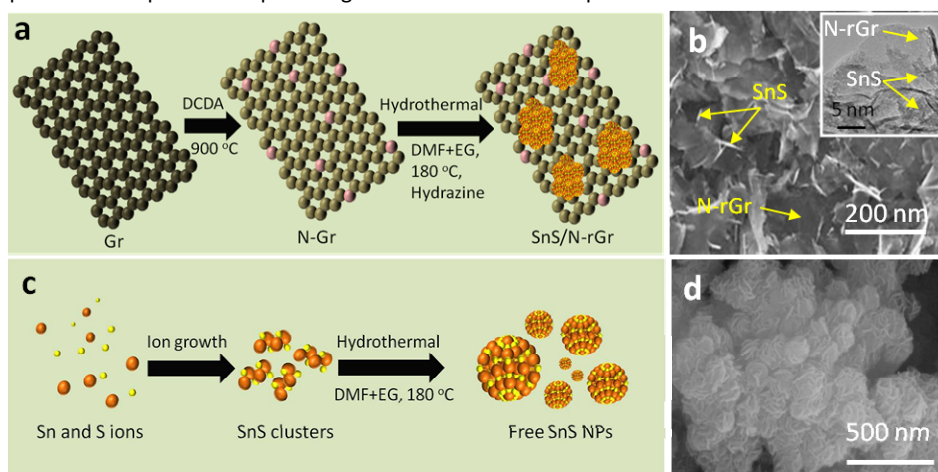

Fig. 1 Synthesis of SnS through a solution process with and without graphene sheets. (a) Schematic hydrothermal synthesis process of SnS/N-rGr hybrid. (b) SE image of the SnS/N-rGr hybrid; the inset shows the corresponding TEM image (Well dispersed nanosheets of SnS grown on N-rGr). (c) Schematic hydrothermal synthesis process of free SnS particles. (d) SEM image of the free SnS particles.
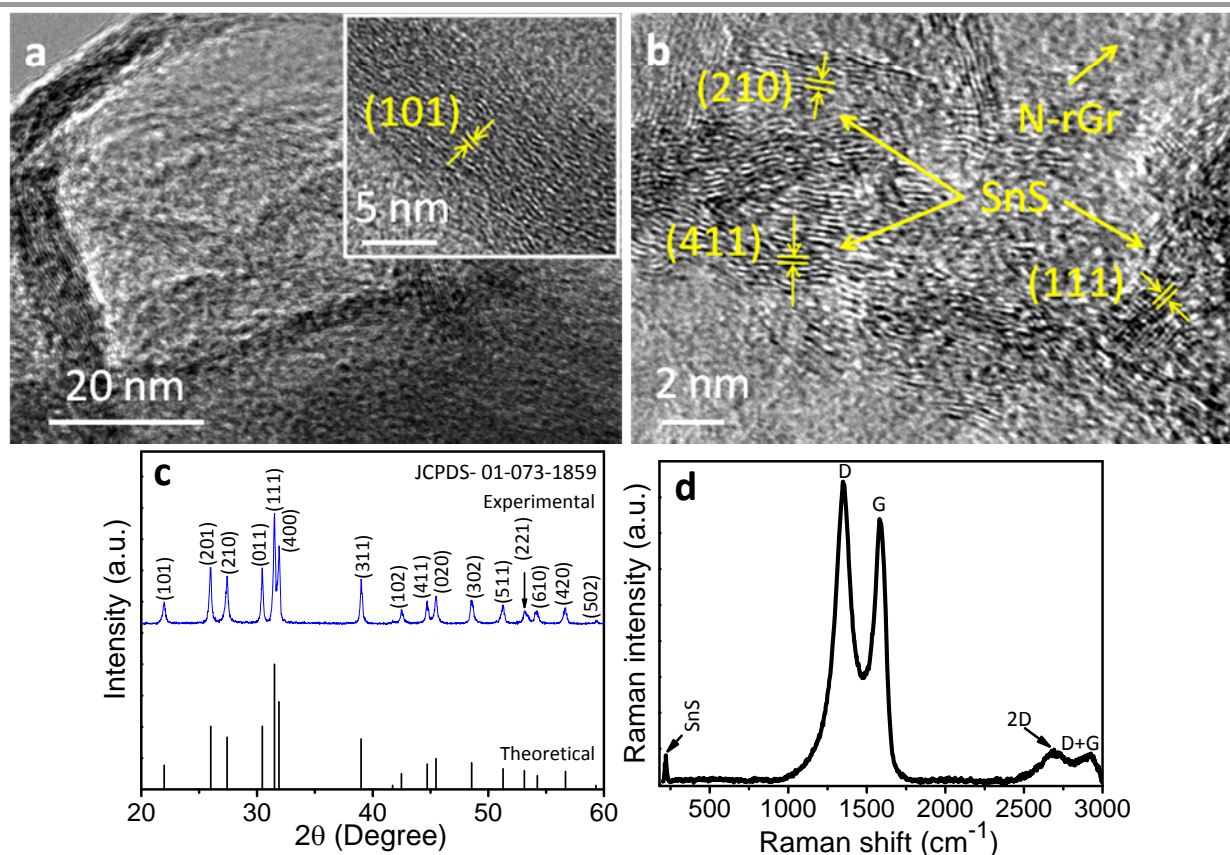
Fig. 2 (a) TEM image showing the folded edges of the SnS particles on N-rGr in the hybrid. The inset shows a magnified image of the folded edges of the SnS particle (b) High-resolution TEM image showing SnS with highly exposed edges stacked on the N-rGr sheet. (c) Experimental and theoretical XRD patterns d) Raman spectrum of the SnS/N-rGr hybrid showing the SnS at 221 cm^{-1}, D band at 1355 cm^{-1} and G band at 1582 cm^{-1}.

A remarkable difference in morphology denotes the significant function of doped graphene as a novel support material for mediation of nanomaterial growth. Elemental mapping of the SnS/N-rGr hybrid demonstrated that the carbon, tin, sulfur, and nitrogen were homogeneously distributed in the sample, and the 2D-SnS-nanosheets were very effectively combined with the N-rGr nanosheets (see ESI, Fig. S2). The corresponding elemental compositions exhibited an atomic ratio of C : N : Sn : S (63.20 : 2.18 : 17.30 : 17.32), consistent with the XPS results. Raman spectroscopy revealed characteristic peaks of SnS at 221 cm^{-1} and D,

G, 2D and D+G bands of graphene in the hybrid (Fig. 2d). The X-ray photoelectron spectroscopy (XPS) analysis of the SnS/N-rGr hybrid exhibited an elemental composition of 63.26 at% C, 17.28 at% Sn, 17.31 at% S, and 2.15 at% N (see ESI, Fig. S3). Importantly, the N-rGr sheets provided a novel substrate for the nucleation and subsequent growth of SnS. The growth of SnS was found to be perceptive to N-rGr with tiny free particles grown in solution. This perceptive growth was ascribed to the relations between functional groups on the N-rGr sheets and SnS precursors in a suitable solvent environment.[16]
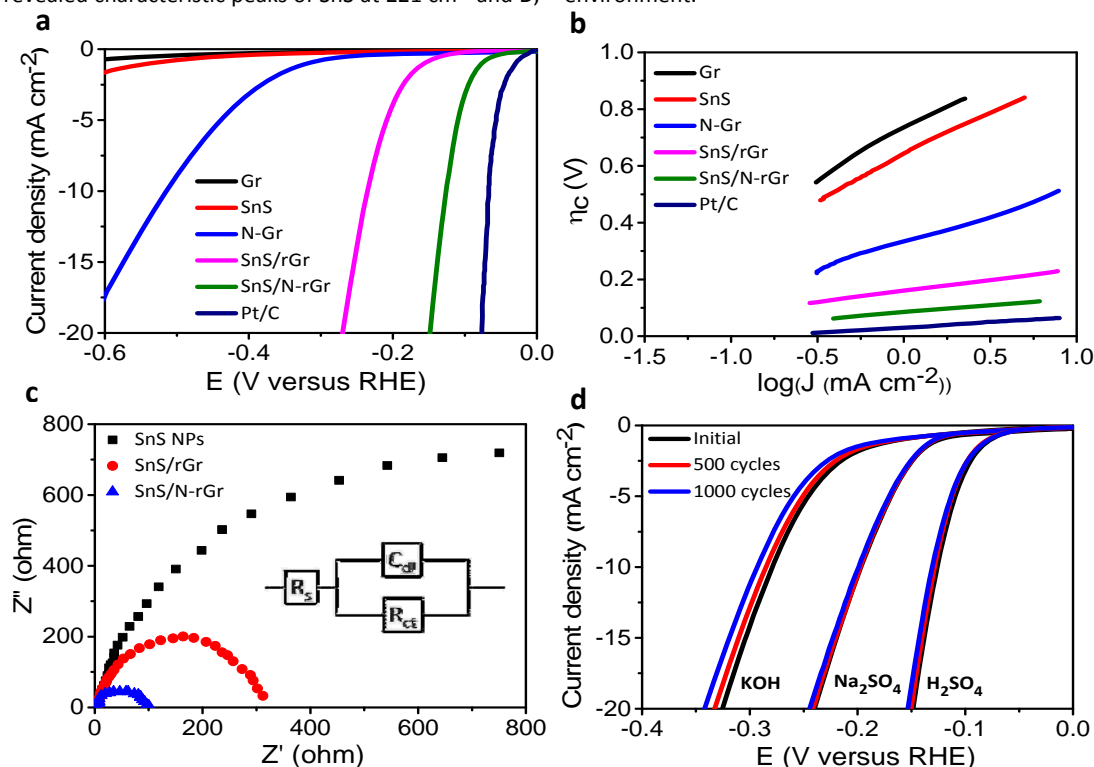
Fig. 3 (a) HER polarization curves of various hybrid electrocatalysts in 0.5 M H_2SO_4; (b) corresponding Tafel plots. (c) Electrochemical impedance spectroscopy data for various catalysts in 0.5 M H_2SO_4; data were collected for the electrodes under the HER overpotential of 100 mV. Inset shows the equivalent circuit diagram. (d) Polarization data for SnS/N-rGr hybrid in 0.5 M H_2SO_4, 0.5 M Na_2SO_4 and 0.1 M KOH initially and after 500 and 1000 potential sweeps.

We evaluated the electrocatalytic HER activities of the SnS/N-rGr hybrid catalyst deposited on a glassy carbon electrode in 0.5 M H_2SO_4 solution using a typical three-electrode configuration at a constant active mass loading in order to compare with a commercial Pt/C catalyst (Fig. 3a). Individual free SnS nanoparticles or graphene exhibited only weak HER activity; on the contrary, the HER activity of the SnS/rGr hybrid catalysts was higher than that of the free SnS particles. As shown in Fig. 3a, the SnS/N-rGr hybrid catalyst produced small onset overpotential of -125 mV for the HER (beyond which the cathodic current density rapidly increased under more negative potentials). Note that the onset overpotential of the SnS/N-rGr hybrid was smaller than that of SnS/x-rGr hybrids (x = P, Se), which suggests prominent catalytic activity of the SnS/N-rGr hybrid for HER (see ESI, Fig. S4). Also the HER activity of SnS/N-rGr hybrid catalysts was better than SnS/CNT and SnS/N-CNT catalysts (Fig. S4) suggesting the enhancement in HER strongly depend on the interface with carbon materials. Tafel plots (η vs log j) obtained from the overpotentials versus logarithmic current density are

shown in Fig. 3b and are useful for quantitative kinetic analysis of the HER.[17] Tafel slopes are determined by fitting the linear portion of the Tafel plots to the Tafel equation (η = b log j + a, where j is the current density, a is the empirical coefficient & b is the Tafel slope). The Tafel plots revealed Tafel slopes of 30, 38 and 266 mV/dec for Pt/C, SnS/N-rGr and free SnS catalyst, respectively. The overall HER mechanism in acidic media occurred via three possible steps. The first step is a primary discharge step $[H_3O^+ + e^- \rightarrow H_{ads} + H_2O]$ (Volmer reaction), Tafel slope ~120 mV/dec], while the second is an electrochemical desorption step $[H_{ads} + H_3O^+ + e^- \rightarrow H_2 + H_2O$ (Heyrovsky reaction), Tafel slope ~40 mV/dec], and the third is a recombination step $[H_{ads} + H_{ads} \rightarrow H_2$ (Tafel reaction), Tafel slope ~30 mV/dec].[18] The determined Tafel slope of 38 mV/dec implied that electrochemical desorption is a rate-determining step with the Volmer–Heyrovsky mechanism for HER. The exchange current density (i_0) was calculated to be 6.23 mA/cm^2. The superior catalytic behaviour of the SnS/N-rGr hybrid might have arisen from the

synergetic effect between the exposed active edge sites and good conductive pathways supplied by the SnS/N-rGr hybrid. The observed HER activity (i.e., onset overpotential, Tafel slopes) compares favourably to the behaviours of other non-Pt nanostructured HER catalysts such as MoS_2, Mo_2C, Ni_2P, MoS_2/rGr, CoP, CoP/CNT, MoP, Ni_xS_y, and Ni-Mo-N nanosheets (Table S1).[8, 10a, 12a, 19] To obtain further insight into the intrinsic catalytic activity of SnS/N-rGr, the turnover frequency (TOF) for each active site was calculated.[20] The number of active sites was examined first by CV in H_2SO_4 at a scan rate of 50 mV/s. Fig. S5 shows the current vs. voltage (CV) plot of the SnS/N-rGr hybrid catalyst. No apparent redox peaks or large current were observed, indicating good ion transport in the SnS/N-rGr hybrid. The number of active sites on the prepared hybrid catalyst was calculated to be 4.48×10^{-8} mol. This prepared catalyst achieved a TOF of 0.23 s^{-1} at a -125 mV overpotential, assuming all surface sulfur sites participated in the HER catalysis. These values were comparable to those of several non-noble metal based catalysts.[8,21] In addition, the Faraday yield of hydrogen production was calculated and was approximately 99% for 10 min of electrolysis (see ESI, Fig. S6).

The high performance of our SnS/N-rGr hybrid in the HER was thought to stem from the strong chemical/electronic coupling between SnS and N-rGr sheets. Chemical interactions led to perceptive growth of highly dispersed SnS nanoparticles on the N-graphene, which was free of aggregation. The small size and high dispersion of SnS on graphene yielded numerous available edges that could serve active catalytic sites for HER. Electronic coupling to the underlying graphene sheets in an interrelated conducting system provided rapid electron transport from the highly resistive SnS nanoparticles to the electrodes. To analyze this effect, we demonstrated electrochemical impedance measurements (EIS) at an overpotential of η = 0.10 V with an electrical equivalent circuit diagram, as shown in Fig. 3c. The SnS/N-rGr hybrid exhibited a Faradaic impedance or charge-transfer impedance, R_{ct} (98 Ω), that was much lower than that of the free SnS particles (2 kΩ). It has been established that R_{ct} is closely related to the electrocatalysis kinetics, and a lower R_{ct} value corresponds to a faster reaction rate. Furthermore, the small series resistance values observed for all samples (~4.4–5.5 Ω) manifests the good conductivity of the electrolyte. Thus, the fast charge transfer during the electrocatalytic reaction coupled with a large exposed active surface area could have contributed to the superior electrocatalytic activity of the SnS/N-rGr hybrid. We cycled our SnS/N-rGr hybrid catalyst continuously for 500 and 1000 cycles in H_2SO_4. At the end of cycling, the catalyst showed similar I-V curves to those found earlier, along with a negligible loss of cathodic current (Fig. 3d). The SnS/N-rGr hybrid also catalyzed the HER in neutral and alkaline solutions, exhibiting overpotentials of -196 and -279 mV at a cathodic current density of 10 mA/cm^2 (Fig. 3d). However, the HER performance of the SnS/N-rGr hybrid deteriorated significantly when increasing the overpotential by 17 mV in KOH after 1000 cycles due to catalyst poisoning or delamination. In addition, the SnS/N-rGr hybrid catalyst was able to maintain a stable HER current density of ~10 mA/cm^2 for ~500 min at a constant voltage of -0.13 V versus RHE in 0.5 M H_2SO_4 (see ESI, Fig. S7). The excellent activity, physical and chemical stability (Figs. S8 and S9), cost-effectiveness, and corrosion-resistance strongly support the SnS/N-rGr hybrid catalyst as a new HER catalyst to replace precious Pt catalysts for various applications such as water electrolysis, fuel cells and batteries.

Conclusions

In summary, we present the first demonstration of scalable synthesis of a low-cost highly-efficient SnS/N-rGr hybrid catalyst via a facile hydrothermal approach. With highly exposed edges and excellent electrical coupling to the underlying doped graphene, the SnS/N-rGr hybrid catalyst exhibited high HER activity with a low overpotential of -0.125 V, Tafel slope of ~38 mV/dec, large cathodic currents and high long-term durability in acid, base and neutral media. The observed Tafel slope suggests that electrochemical desorption is the rate limiting step and Volmer–Heyrovsky mechanism suitable for the HER. The advanced SnS/N-rGr hybrid could be promising alternate to replace precious metal catalysts for clean H_2 production in practical applications.

Acknowledgements

Notes and references

1   M. Walter, E. Warren, J. McKone, S. Boettcher, Q. Mi, E. Santori, N. Lewis, *Chem. Rev.,* 2010, **10,** 6446.
2   (a) M. Gong, W. Zhou, S. Pennycook, B. Hwang, H. Dai, *Nat. Commun.* 2014, **5,** 4695; (b) S.S. Shinde, A. Sami, J.H. Lee, *J. Mater. Chem. A,* 2015, **3,** 12810.
3   X. Chen, D. Wang, Z. Wang, P. Zhou, Z. Wu and F. Jiang, *Chem. Commun.,* 2014, **50,** 11683.
4   (a) H. Tang, K. Dou, C. Kaun, Q. Kuang, S. Yang, *J. Mater. Chem. A,* 2014, **2,** 360; (b) M. Faber, M. Lukowski, Q. Ding, N. Kaiser, S. Jin, *J. Phys. Chem. C,* 2014, **118,** 21347.
5   V. Jovic, U. Lacnjevac, B. Jovic, N. Krstajic, *Electrochim. Acta.* 2012, **63,** 124.
6   W. Chen, K. Sasaki, C. Ma, A. Frenkel, N. Marinkovic, J. Muckerman, Y. Zhu, R Adzic, *Angew. Chem. Int. Ed.,* 2012, **51,** 6131.
7   H. Vrubel, X. Hu, *Angew. Chem., Int. Ed.* 2012, **51,** 12703.
8   E. Popczun, J. McKone, C. Read, A. Biacchi, A. Wiltrout, N. Lewis, R. Schaak, *J. Am. Chem. Soc.,* 2013, **135,** 9267.
9   Y. Liu, T. Kelly, J. Chen, W. Mustain, *ACS Catal.,* 2013, **3,** 1184.
10 (a) D. Wang, M. Gong, H. Chou, H. Dai, *J. Am. Chem. Soc.* 2015, **137,** 1587; (b) D. Li, U. Maiti, J. Lim, D. Choi, W. Lee, Y. Oh, G. Lee, S. Kim, *Nano Lett.,* 2014, **14,** 1228;
11 S. Shima, O. Pilak, M. Stagni, W. Meyer-Klaucke, E. Warkentin, R. Thauer, U. Ermler, *Science,* 2008, **321,** 572.
12 (a) W. Chen, C. Wang, W. Xu, J. Muckerman, Y. Zhu, R. Adzic, *Energy Environ. Sci.,* 2013, **6,** 943; (b) G. Yue, J. Wu, Y. Xiao,

M. Huang, J. Lin, J. Lin, *J. Mater. Chem. A,* 2013, **1,** 1495; (c) Q. Jiang, G. Li, X. Gao, *Chem. Commun.,* 2009, 6720.

13 (a) J. Seo, J. Jang, S. Park, C. Kim, B. Park, J. Cheon, *Adv. Mater.,* 2008, **20,** 4269; (b) Y. Zou, Y. Wang, *ACS Nano,* 2011, **5,** 8108.

14 (a) X. Huang, X. Qi, F. Boey, H. Zhang, *Chem. Soc. Rev.,* 2012, **41,** 666; (b) M. Sathish, S. Mitani, T. Tomai, I. Honma, *J. Phys. Chem. C,* 2012, **116,** 12475.

15 (a) Y. Jiao, Y. Zhu, L. Li, Y. Han, Y. Chen, A. Du, M. Jaroniec, S. Qiao, Nature Commun. 2014, **3,** 3783; (b) J. Jin, X. Fu, Q. Liu, J. Zhang, J. Mater. Chem. A 2013, **1,** 10538; (c) Z. Liu, F. Peng, H. Wang, H. Yu, W. Zheng, J. Yang, Angew. Chem., Int. Ed. 2011, **50,** 3257.

16 H. Wang, J. Robinson, G. Diankov, H. Dai, *J. Am. Chem. Soc.,* 2010, **132,** 3270.

17 T. Jaramillo, K. Jorgensen, J. Bonde, J. Nielsen, S. Horch, I. Chorkendorff, *Science,* 2007, **317,** 100.

18 B. Conway, B. Tilak, *Electrochim. Acta,* 2002, **47,** 3571.

19 D. Chung, J. Han, H. Lee, Y. Sung, *Nanoscale,* 2015, **7,** 5157.

20 D. Merki, S. Fierro, H. Vrubel, X. Hu, *Chem. Sci.,* 2011, **2,** 1262.

21 (a) J. Xie, H. Zhang, Y. Xie, *Adv. Mater.,* 2013, **25,** 807; (b) J. McKone, N. Lewis, H. Gray, *ACS Catal.,* 2013, **3,** 166.